Pressure-induced metallization in the absence of a structural transition in the layered ferromagnetic insulator $Cr_2Ge_2Te_6$

Weizhao Cai [1,2,*] Luo Yan,[3] Su Kong Chong,[2] Jingui Xu,[4]
Dongzhou Zhang,[4] Vikram V. Deshpande,[2] Liujiang Zhou [3,†] and Shanti Deemyad [2,‡]
[1]*School of Materials and Energy, University of Electronic Science and Technology of China, Chengdu 611731, Sichuan, China*
[2]*Department of Physics and Astronomy, University of Utah, Salt Lake City, Utah 84112, USA*
[3]*School of Physics, University of Electronic Science and Technology of China, Chengdu 611731, Sichuan, China*
[4]*PX2, Hawaii Institute of Geophysics and Planetology, University of Hawaii at Manoa, Honolulu, Hawaii 96822, USA*

(Received 27 April 2022; accepted 27 July 2022; published 9 August 2022)

We report the crystallographic and electrical transport properties of single crystals of the ferromagnetic two-dimensional (2D) material $Cr_2Ge_2Te_6$ under high pressure. In contrast to previous studies, our high-pressure single-crystal x-ray diffraction under hydrostatic conditions shows prominent anisotropic compressibility in the layered structure of the crystalline $R\bar{3}$ phase of $Cr_2Ge_2Te_6$ without any structural phase transitions up to 20 GPa. Our data confirm a distinct and irreversible crystalline-amorphous transformation in $Cr_2Ge_2Te_6$. The loss of crystallinity starts at 20 GPa; however, the crystalline phase and amorphous state coexist even at the maximum pressure of 31.2 GPa. High-pressure powder x-ray diffraction data and electrical resistivity measurements of $Cr_2Ge_2Te_6$ using NaCl as the pressure-transmitting medium reveal an insulator-to-metal transition in the absence of a phase transition at ∼3.9 GPa; at a considerably lower pressure than the previously reported (7–14 GPa). Density functional theory calculations demonstrate the density of states around the Fermi level are primarily dominated by Cr 3*d* and Te 5*p* states. Hence the large reduction of Cr-Te bond lengths within the $CrTe_6$ octahedra under compression is most likely responsible for the band-gap closure. This study clarifies that the phase stability and onset of metallization pressure in the $Cr_2Ge_2Te_6$ sample are sensitive to the hydrostatic environments and demonstrates how pressure can be used to tune the physical properties of 2D ferromagnetic compounds.

DOI: 10.1103/PhysRevB.106.085116

I. INTRODUCTION

The discovery of magnetism in two-dimensional (2D) materials with layers interlinked through van der Waals (vdW) interactions has attracted intense interest due to their potential applications in new spintronics, multiferroics, and even the possibility of discovering new physics such as Kitaev quantum spin liquid states [1,2]. Ferromagnetic insulators such as chromium trihalides CrX_3 (X = Br and I) and ternary chromium-based tritellurides $Cr_2Z_2Te_6$ (Z = Si and Ge) are a few typical vdW materials that demonstrate ferromagnetic order from bulk crystals to monolayer limit [3,4]. In the layered structure of CrX_3, the Cr^{3+} cations within the layers adopt a honeycomb network of edge-sharing CrX_6 octahedra character [5]. The CrI_3 has the largest magnetic ordering temperature T_c of 68 K among the chromium trihalides, and the ferromagnetic order is maintained even down to monolayer with temperatures as high as 45 K [6,7]. In contrast to CrX_3, ternary compounds $Cr_2Z_2Te_6$ (Z = Si and Ge) possess a similar layered crystal structure, with the center of the honeycomb network occupied by Ge_2 dimers [8]. The Curie temperature T_c increases from 32 K for $Cr_2Si_2Te_6$ to 66 K for $Cr_2Ge_2Te_6$ [9–11]. As a Heisenberg's 2D ferromagnet with strong magnetic anisotropy, the monolayer of $Cr_2Ge_2Te_6$ is primarily single ion anisotropy, but its Curie temperature drops to 22 K [4].

Application of high pressure is an efficient route to regulate the electronic and magnetic properties of 2D vdW compounds. For example, pressure has been successfully used to control the magnetism in both samples of a few atomic layers and bulk single crystals of CrI_3 [12–14]. Cr-based vdW charge transfer insulators, $Cr_2X_2Te_6$ (X = Si and Ge), with ferromagnetic ground state are promising 2D materials for exploring the interplay between magnetic and electrical properties and have been the subject of many recent studies. A recent study on $Cr_2Si_2Te_6$ demonstrated concurrent structural phase transition and insulator-metal transition followed by superconductivity at ∼7.5 GPa [15], while in $Cr_2Ge_2Te_6$, no superconductivity was observed at comparable pressure [16]. Recent studies reveal that the Curie temperature T_c of $Cr_2Ge_2Te_6$ decreases by about 18% between 0 and 4.5 GPa; however, upon further pressurization the T_c starts to increase and $Cr_2Ge_2Te_6$ transforms from a ferromagnetic insulator to a correlated 2D Fermi metal at 7.0 GPa with T_c exceeding ∼250 K at 9.1 GPa [17–19]. Understanding the origin of these drastic electronic effects requires investigating the pressure effects on the crystal structures of $Cr_2Ge_2Te_6$. The phase stability of $Cr_2Ge_2Te_6$ has been studied using high-pressure powder x-ray diffraction and Raman spectroscopy, but the observations were inconsistent when different pressure-transmitting media (PTM) were utilized [20–22]. These inconsistencies prompt us to investigate the structural stability and the

*Corresponding author: wzhcai@uestc.edu.cn
†Corresponding author: Ljzhou86@uestc.edu.cn
‡Corresponding author: Deemyad@physics.utah.edu

onset metallization pressure of $Cr_2Ge_2Te_6$ under hydrostatic pressure.

In this work, we study the structural and electronic properties of $Cr_2Ge_2Te_6$ single crystals using high-pressure synchrotron single-crystal x-ray diffraction and electrical resistance measurements in diamond-anvil cells together with first-principles calculations. Using helium as the PTM in the x-ray measurements, we accurately determined the crystal structures of $Cr_2Ge_2Te_6$ under high pressure and in contrast to previous studies we show that there is no phase transition below ∼20.0 GPa. Further compression leads to an irreversible amorphization in $Cr_2Ge_2Te_6$. Electrical transport measurements showed that a complete insulator-metal transformation occurred at ∼3.9 GPa in $Cr_2Ge_2Te_6$, which is much lower than the previously reported values of 7–14 GPa. Density functional theory (DFT) calculations reveal a distinct insulator-to-metal transition which takes place at 3.2 GPa, consistent with our experiments, and suggest that a large reduction of Cr-Te bond lengths within $CrTe_6$ octahedra is most likely responsible for the band-gap closure.

II. EXPERIMENTAL AND THEORETICAL METHODS

A. Synthesis of $Cr_2Ge_2Te_6$ single crystals

The $Cr_2Ge_2Te_6$ single crystals are grown by the self-flux method [23]. The starting materials of 2 mmol of Cr (99.999%; Sigma Aldrich) and 2 mmol Ge (99.999%; Sigma Aldrich) powders were initially mixed with the molar ratio of 1:1, and an excess of 24 mmol of Te powder was used as the flux. The mixture was loaded and flame-sealed in a silica ampule under high vacuum pressure of 10^{-5} Pa. The mixture was heated at 700 °C for 2 wk and slowly cooled to 500 °C with a rate of 5 °C/h and then excess Te was removed by the centrifugation process. Finally, platelike single crystals with a silvery luster were obtained. The sample purity was confirmed both by single-crystal and powder x-ray diffraction.

B. High-pressure x-ray diffraction measurements

The Boehler-Almax plate diamond-anvil cells (DACs) with 500 μm culet size and a large opening angle of ∼60 ° were used in the high-pressure single-crystal x-ray measurements. Pressure was calibrated by the ruby fluorescence method and was measured before and after each diffraction data collection [24].

Unlike the previous experiments, in which the 4:1 methanol-ethanol mixture [21] and silicone oil [22] were used as pressure-transmitting media, we chose the helium (He) as the pressure-transmitting medium (PTM). A plate-shaped single crystal of $Cr_2Ge_2Te_6$ with the dimension of $\sim 28 \times 25 \times 10\,\mu m^3$ was loaded in the ∼220-μm diameter and ∼65-μm thickness rhenium gasket chambers. The high-pressure single-crystal x-ray data were collected up to 19.5 GPa, above which only powder diffraction data were recorded at room temperature. For data above 20 GPa, only powder x-ray diffraction from the wide φ angle scan was collected, and cleaned XRD patterns data were obtained by removing the background (gasket and solid helium and diamond) [25].

All high-pressure single-crystal x-ray diffraction data of $Cr_2Ge_2Te_6$ were collected at 13-BM-C beamline, GSECARS of the Advanced Photon Source (APS), Argonne National Laboratory with x-ray wavelength of 0.4341 Å. Single-crystal diffraction data were recorded using a PILATUS3 1M (Dectris) detector. The exposure time was set as 1 s/deg, and each diffraction image covered 1 ° on the φ axis. The collected x-ray data were indexed and reduced using the APEX3 package. The crystal structures of $Cr_2Ge_2Te_6$ can be solved by the direct method using SHELXS-97 [26] and refined with SHELXL interfaced by OLEX2-1.5 [27]. All the Cr, Ge, and Te atoms were refined anisotropically. The selected crystallographic parameters and structure information were summarized in Supplemental Material Tables S1 and S2, respectively [28].

In order to examine the phase stabilities of the ambient-pressure structure and mimic identical hydrostatic conditions of electrical transport measurements, additional high-pressure synchrotron powder x-ray measurements of $Cr_2Ge_2Te_6$ were performed using NaCl as the PTM. The x-ray data at room temperature were collected at 16-ID-B, HPCAT, APS ($\lambda = 0.4246$ Å). The diffraction images were integrated using the DIOPTAS 0.5.1 software [29], and x-ray data were fitted by the Le Bail fitting method using the GSAS-EXPGUI package [30], and the single-crystal structures of $Cr_2Ge_2Te_6$ were used as the starting models to carry out all the data refinements.

C. High-pressure electrical transport measurements of $Cr_2Ge_2Te_6$ single crystal

High-pressure electrical resistance measurements of $Cr_2Ge_2Te_6$ single crystal were conducted by a four-terminal method. A fine mixture of alumina powder and epoxy was used to insulate the electrodes and gasket. A 500-μm culet size DAC was used for all the measurements. Stainless steel gaskets with an ∼300 μm hole were filled with the alumina-epoxy mixture and compressed to ∼7.0 GPa and then released to ambient pressure. And an ∼130-μm hole was laser-drilled in the compressed insulated gasket. Fine NaCl powder was inserted in the hole acting as the pressure medium and the powder was initially compressed to ∼2.0 GPa until it turned transparent. A platelike $Cr_2Ge_2Te_6$ single crystal was carefully loaded on top of the compressed NaCl, and four platinum electrodes with the thickness of 5 μm were arranged to contact the sample. The dc electrical resistivity of the sample was measured using a current of 50–200 μA. A closed-cycle helium cryostat was employed to examine the temperature dependence of the electrical resistance at specific pressures in the range of 2.4–300 K. Pressure was determined using the ruby fluorescence method both at room temperature and a low temperature of ∼4.0 K with the aid of an online ruby system.

D. Electronic structure calculations

The electronic structure calculations of $Cr_2Ge_2Te_6$ were performed using DFT based on the projector augmented wave method, as implemented in the Vienna *ab initio* simulation package (VASP) [31]. The exchange-correlation interactions were depicted within the generalized gradient approximation (GGA) [32,33] as formulated by Perdew-Burke-Ernzerhof [34]. The plane-wave cutoff energy of 450 eV and the Γ-central $9 \times 9 \times 3$ k-point mesh were adopted. The high-

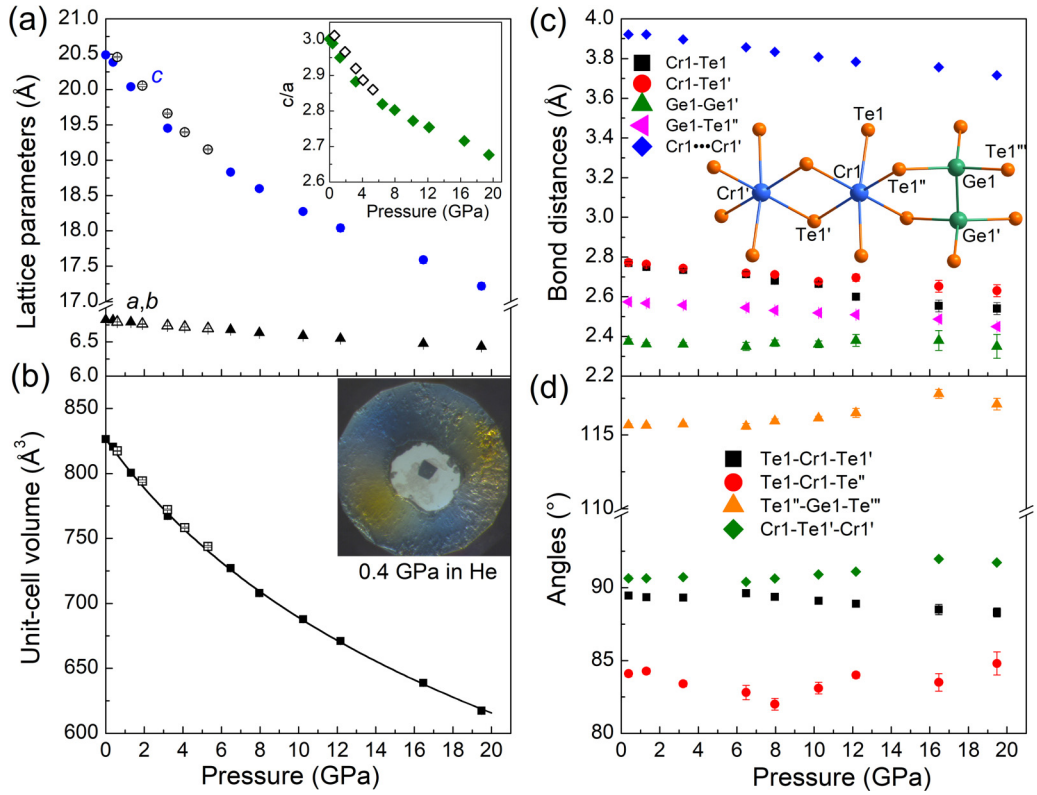

FIG. 1. (a) Lattice parameters of $Cr_2Ge_2Te_6$ as a function of pressure. The inset indicates the pressure dependence of the c/a ratio. (b) The third-order Birch-Murnaghan equations of states fit the unit-cell volume data. The inset displays a bulk single crystal of $Cr_2Ge_2Te_6$ compressed in helium at 0.4 GPa. The powder x-ray data using NaCl as the PTM are indicated as unfilled symbols. (c) Changes in bond distances under compression. The coordination environments of Cr1 and Ge1 atoms are shown in the inset. (d) Evolution of Te-Cr-Te and Te-Ge-Te angles under pressure.

symmetry path used in band structure calculations is set along Γ-*A*-*H*-*K*-Γ-*M*-*L*-*H*, and the high-symmetry points Γ, *A*, *H*, *K*, *M*, and *L* are (0,0,0), (0,0,0.5), (0.333,0.667,0.5), (0.333,0.667,0), (0,0.5,0), and (0,0.5,0.5), respectively. The Cr $3d^5 4s^1$, Ge $4s^2 4p^2$, and Te $5s^2 5p^4$ electrons were treated explicitly in all calculations. In addition, the effective value of $U = 1.0$ eV was utilized to treat the on-site Coulomb interaction of localized electrons [35]. An electron localization function (ELF) was calculated to describe and visualize chemical bonds in the $Cr_2Ge_2Te_6$ structures at selective pressures [36]. To avoid the error induced from computational methods and match the experimental results, we performed DFT calculations using the experimental lattice parameters and only relaxed the atomic positions within lattices in all DFT calculations. The force per atom was set to be less than 0.01 eV/Å.

III. RESULTS AND DISCUSSION

A. Structure evolution under pressure

The crystal structures of $Cr_2Ge_2Te_6$ under high pressure were determined by the synchrotron x-ray diffraction method at room temperature. Unlike the previous powder x-ray diffraction experiments, in which silicone oil or a 4:1 methanol-ethanol mixture was employed as the PTM [19,22], in our work, we used helium (He) as the PTM for all the diffraction experiments, since helium was proved to be one of the best PTM and it could provide good hydrostaticity at least to 20 GPa [37]. As shown in Fig. 1, we did not observe a crystalline-crystalline structure phase transition through the whole range from ambient pressure to ~20 GPa. Above ~20 GPa, the $Cr_2Ge_2Te_6$ sample starts undergoing a crystalline-amorphous transition, which hampers the determination of the lattice parameters. With pressure increased to 31.2 GPa, the intensities of reflections (spots) from the sample are much weaker than that at 19.5 GPa and the diffraction peaks become wider (e.g., 8 °–10 °). These indications reveal the sample gradually amorphized under compression and it still maintains its crystallinity partially at 31.2 GPa. Hence the crystalline phase coexists with the amorphous state at 31.2 GPa. A complete amorphization could be expected to be observed at even much higher pressures (see Supplemental Material Figure S1 [28]). In the previous reports using a silicone oil/methanol-ethanol mixture as the pressure media, a new phase II was detected above 7.0/14.0/18.3 GPa [19,21,22]; we attribute the origin of these discrepancies to the presence of deviatoric stress which especially can be prominent in 2D materials [38]. Interestingly, in our powder x-ray diffraction studies using NaCl as the PTM, no phase transition occurred up to 5.2 GPa at room temperature, well consistent with the previous reports (Fig. S2). It is well known that the XRD patterns are commonly broadened under non-/quasihydrostatic environments; these wide diffraction peaks may provide fake information for the identification of a new phase [39]. As shown in Fig. 1(a), the lattice parameters of

$Cr_2Ge_2Te_6$ shrink monotonically with increasing pressure; the c axis has the largest compressibility due to the compressible vdW interactions, while the a and b axes are very rigid within the layers. For example, the c axis is reduced by ∼16.0% up to 19.5 GPa, while the a and b axes decrease almost three times smaller: only compressed by ∼5.7%. It is obvious that the [001] is the soft direction, which is well consistent with the 2D layered structure. As shown in Fig. 1(b), the unit-cell volume decreases gradually with increasing pressure, indicative of no phase transition occurring up to ∼20 GPa. The results indicate that the ambient-pressure phase of $Cr_2Ge_2Te_6$ is robust against pressure before the amorphization. The volume data $V(P)$ can be well fitted by the third-order Birch-Murnaghan equation of state, the zero-pressure bulk modulus B_0 is 39.2(13) GPa, and its pressure derivative B' equals 3.8(3). The magnitude of B_0 is comparable to the analogous compound $Cr_2Si_2Te_6$ [37(1) GPa] [40].

At ambient conditions, the structure of $Cr_2Ge_2Te_6$ adopts a typical lamellar structure type, with one Cr, one Ge, and one Te atom in the asymmetric unit [11,41]. The structure features a rhombohedral system with space group $R\bar{3}$ and $Z = 3$. The edge-sharing $CrTe_6$ octahedra form a honeycomb network with the remaining free spaces of the center occupied by Ge_2 dimers, and these layers are interacted with weak vdW interactions and packed along the c axis [Fig. 2(a)]. It can be easily seen that the structure of $Cr_2Ge_2Te_6$ is derived from the known ferromagnetic insulator CrI_3, in which the positions of Ge_2 dimers are absent [5]. The Cr1 atom adopts an octahedral geometry and is coordinated to six Te1 atoms and these octahedra are interconnected via an edge-sharing manner [Fig. 2(c)]. From the single-crystal x-ray data refinements, the atomic coordinates of Cr, Ge, and Te under high pressure are accurately determined, which allows us to analyze the detailed structural evolution under compression. The Cr1-Te1 bond distance shrinks from 2.769(7) Å at 0.4 GPa to 2.54(3) Å at 19.5 GPa, while the Te1-Cr1-Te1′ angle decreases slightly from 89.46(7)° to 88.3(3)°. The Cr1···Cr1′ distances are shortened from 3.9216(3) to 3.7157(15) Å when pressure increases from 0.4 to 19.5 GPa and the Cr1-Te′-Cr1′ angle changes slightly from 90.65(5)° to 91.73(11)° [Fig. 1(c)]. The Te_3-Ge1-Ge1-Te_3 unit which is parallel to the c axis undergoes slight distortions under compression. For example, the Ge1-Te1″ bond distance decreases from 2.574(2) Å at 0.4 GPa to 2.449(7) Å at 19.5 GPa, while the Ge1-Ge1′ bond lengths are hard to compress, i.e., 2.375(13) Å (at 0.4 GPa) vs 2.35(6) Å (at 19.5 GPa).

B. Pressure-induced insulator-to-metal transition

We also performed electrical transport properties of $Cr_2Ge_2Te_6$ under high pressure on a single-crystal sample with NaCl as the PTM. As shown in Fig. 3(a), the electrical resistance decreases monotonically under compression in the range of crystalline phase $R\bar{3}$. The single-crystal sample shows a distinct insulator behavior at ambient pressure, and its resistance increases rapidly upon cooling. To confirm the onset of the metallization pressure, we measured the temperature dependence of electrical resistance under variable pressures. As shown in Figs. 3(a) and 3(b), the $R(T)$ curve shows negative dR/dT at 0.9 GPa, indicative of semiconductor character.

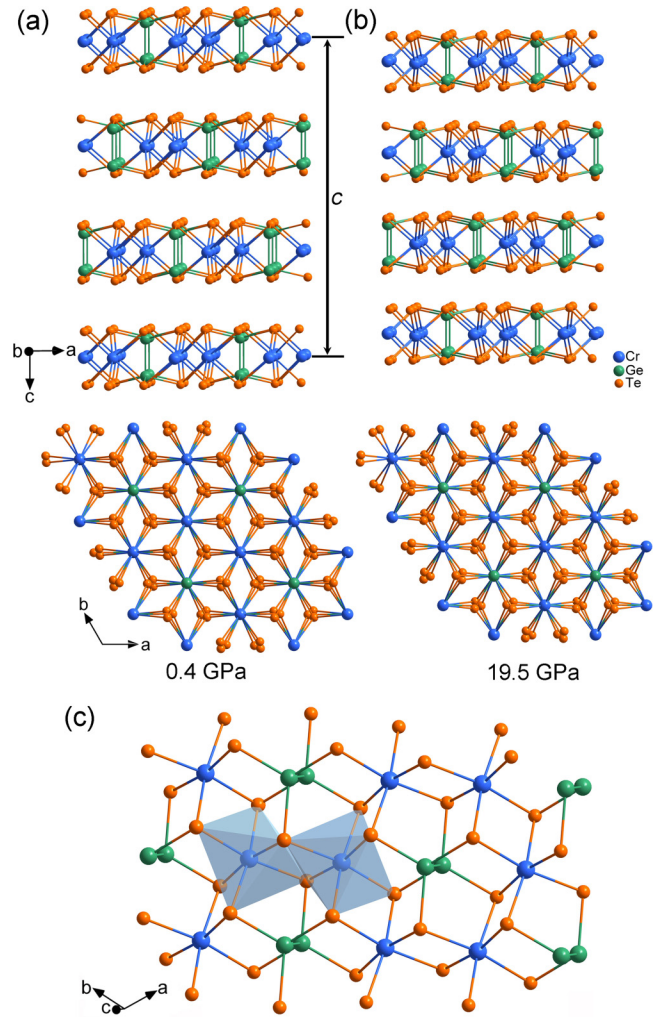

FIG. 2. (a) Crystal structures of $Cr_2Ge_2Te_6$ at 0.4 GPa viewed along the [010] and [001] directions. (b) Structures at 19.5 GPa viewed along the same directions as 0.4 GPa. (c) Single layer of $Cr_2Ge_2Te_6$ viewed approximately along the c axis. The edge-sharing $CrTe_6$ octahedra are indicated.

At 2.2 GPa, the dR/dT demonstrates positive in the high-temperature region, whereas it changes to negative in the low-temperature region, e.g., 40 K at 2.3 GPa. With increasing the pressure to 3.9 GPa, the $dR/dT > 0$ through the whole temperature range of 2.4–300 K, and together with structural data this implies that the sample becomes a 2D metal (Supplemental Material Fig. S2 [28]). The onset of metallization pressure observed here is much lower than the recent report of 7.0 GPa (close to the solidification pressure of the PTM), in which the resistivity measurements were performed in a cubic anvil cell with 1:1 ratio of Flourinert FC70 and FC77 as the PTM [16]. The mixture of FC70 and FC77 has a hydrostatic limit of ∼1.0 GPa, hence quasihydrostatic environments will appear in the range of 1.0–7.0 GPa [42,43]. As discussed above, our powder x-ray diffraction measurements using NaCl as the PTM confirm that no phase transition took place up to 5.2 GPa, hence the semiconductor-to-metal transition of $Cr_2Ge_2Te_6$ is not related to the phase transformation, but to its intrinsic electronic changes. At 3.9 GPa, $R(T)$ follows a power law $R(T) = R_0 + AT^n$ below 30 K, with an exponent

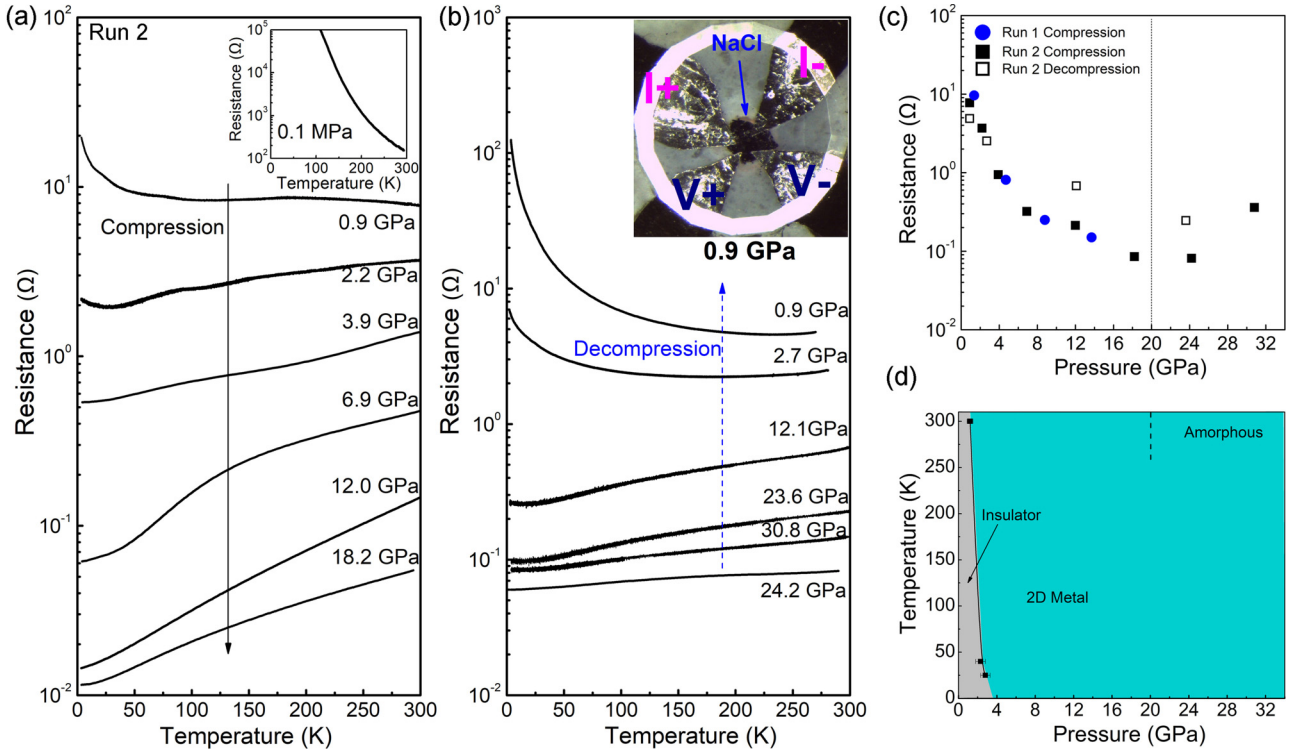

FIG. 3. (a) Electrical resistance of $Cr_2Ge_2Te_6$ in the crystalline phase range (below 20 GPa). The inset indicates the data measured in a different single crystal at ambient pressure. (b) Electrical resistance data in the amorphous phase above 20 GPa. The inset shows the photograph of $Cr_2Ge_2Te_6$ single crystal immersed in the NaCl medium at 0.9 GPa using the four-terminal method for the measurements. (c) Pressure-dependent electrical resistances of $Cr_2Ge_2Te_6$ at room temperature. (d) *P-T* phase diagram $Cr_2Ge_2Te_6$ based on the x-ray and electrical resistance data.

$n \sim 1.95$, an indication of Fermi liquid state (Supplemental Material Fig. S4 [28]). Unlike the previous resistivity measurements within the *ab* plane of $Cr_2Ge_2Te_6$ single crystal, we did not observe an obvious anomaly in electrical resistivity data, which hinders us in tracing the evolution of the Curie temperature under compression [16]. Interestingly, with further increasing the pressure above 3.9 GPa, we did not observe the superconductivity down to 2.4 K prior to the crystalline-amorphous transformation, while in the analogous material $Cr_2Si_2Te_6$, superconductivity emerges at ~7.5 GPa [15]. After pressure releasing from the maximum pressure of 30.8 GPa to 0.9 GPa, we found the $R(T)$ curves are irreversible compared to the initial compression data (e.g., at 0.9 GPa), revealing the crystalline-amorphous transformation could not be recovered; well consistent with the x-ray diffraction data. Like the previous observations [22], the electrical resistance decreases gradually under compression in the crystalline phase, and it goes up after the amorphization occurred above 20 GPa [see Fig. 3(c)]. We constructed the *P-T* phase diagram from the x-ray and electrical resistance data; it can be clearly seen that the metallization pressure increases gradually upon cooling, and the sample undergoes a complete insulator-metal transition around 4.0 GPa below 10 K [see Fig. 3(d)].

C. DFT calculations

To gain insights into the chemical bonding of $Cr_2Ge_2Te_6$, we calculated the ELF at selective pressures (Supplemental Material Fig. S5). The large difference in the ELF between Cr and Te atoms indicates the ionic bonding characteristics, where the charge transfers are from less electronegative Cr to more electronegative Te. There exists a charge localization between Ge-Ge bonds, demonstrating the covalent bonding feature. As shown in Supplemental Material Table S3, we found through Bader charge analysis that the charges on the Cr atom at 0.4 and 19.5 GPa are largely decreased (0.86*e* vs 0.68*e*), revealing that the charge transfer from Cr to Te reduces under compression, whereas the charge on the Ge atom is slightly decreased (0.28*e* vs 0.21*e*).

To better understand the electronic structure evolution of $Cr_2Ge_2Te_6$ under pressure, we performed DFT calculations based on the relaxed structures of experimental single-crystal x-ray data. The calculated band structures of $Cr_2Ge_2Te_6$ at 0.4 GPa indicate that band gap is indirect, with the valence band maximum located at the *A* point and the conduction band minimum settled between the *K* and Γ points [Fig. 4(a)]. The calculated band gap is 0.32 eV at 0.4 GPa, and it decreases to 0.2 eV when the pressure increases to 1.3 GPa. At 3.2 GPa, we observed obvious band-gap closure when the valence bands cross the Fermi level (Supplemental Material Fig. S6 [28]). The insulator-to-metal transition is most likely correlated to the large shrinkage of the Cr-Te bond lengths upon compression [Fig. 1(c)]. The metallization pressure observed here is in good agreement with our electrical transport measurements, but much lower than the previous reports of 7–14 GPa [19,22]. It is notable that in a recent work where the GGA method is used to determine the band gaps of $Cr_2Ge_2Te_6$, the insulator-to-metal transition is calculated to occur at 6.0 GPa, which

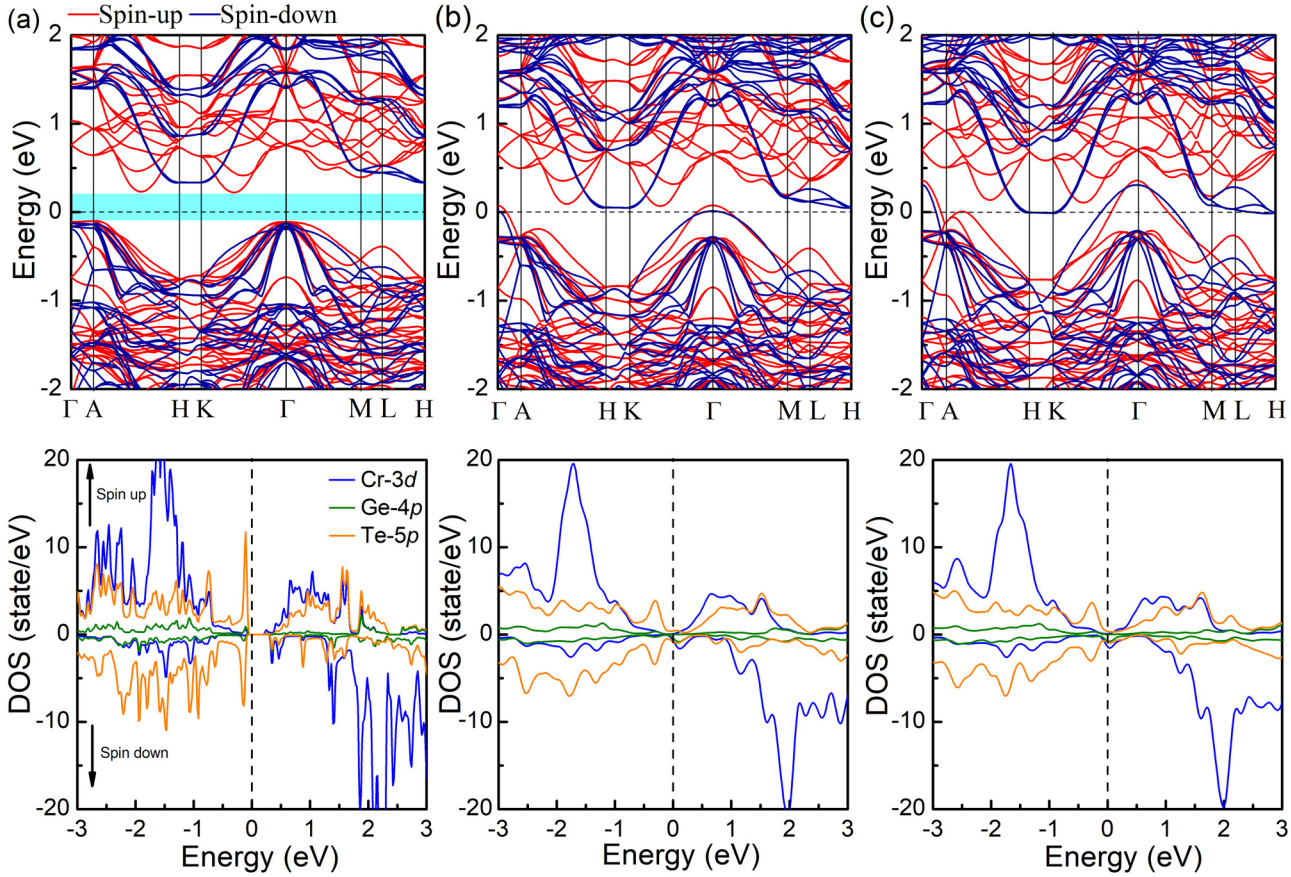

FIG. 4. Calculated electronic band structures and density of states of $Cr_2Ge_2Te_6$ at (a) 0.4 GPa, (b) 3.2 GPa, and (c) 6.5 GPa.

is well consistent with the powder x-ray diffraction measurements performed in the same study under nonhydrostatic conditions (the c/a ratio displays a prominent kink at around 7.5 GPa, indicative of isosymmetric transformation) [19]. In our case, where the $Cr_2Ge_2Te_6$ sample was studied under hydrostatic conditions, it does not undergo phase transition up to 20 GPa, hence the band-gap closure is primarily arising from large reductions of bond lengths. To understand the contributions of the Cr, Ge, and Te orbital states, we plotted the density of states as a function of pressure. Here we compare the partial density of states in three selected pressures of 0.4, 3.2, and 6.5 GPa. At 0.4 GPa, both conduction and valence density of states are mainly occupied by the Cr 3*d* and Te 5*p* states, while the Ge 4*p* states play a minor role in the contributions of the total density of states. The observed *p-d* band gap demonstrates a charge transfer insulator character [Fig. 4(a)] [44]. At 3.2 GPa, the Cr 3*d* and Te 5*p* states cross the Fermi level, indicating metallic character. Unlike the 2D vdW phosphorus trichalcogenides $MnPS_3$, in which the insulator-to-metal transformation generally correlates to the spin state transition and structural transformation with large volume collapse [45]. Moreover, the isostructural compound $Cr_2Si_2Te_6$ exhibits a concurrent insulator-metal transition and structural transition and superconductivity at ∼7.5 GPa [15]. However, in $Cr_2Ge_2Te_6$, the absence of structural transition in the insulator-to-metal transformation implies that pressure modified electronic ground states are purely electronic and the large contraction of Cr-Te bond distances is most likely responsible for the metallization [16].

IV. CONCLUSIONS

In summary, the crystallographic and electrical transport properties of 2D $Cr_2Ge_2Te_6$ single crystal have been investigated by combinations of experimental and DFT calculations. Our high-pressure single-crystal x-ray diffraction measurements using helium as the PTM reveal that the ambient-pressure rhombohedral structure of $Cr_2Ge_2Te_6$ is very robust. The interlayer distances show the largest compressibility along the c axis and there is no phase transition that takes place up to ∼20 GPa. Above 20 GPa, the $Cr_2Ge_2Te_6$ sample starts to lose its crystallinity and the crystalline phase and amorphous state coexist even at the maximum pressure of 31.2 GPa. A prominent insulator-to-metal transition takes place at 3.9 GPa from the electrical transport measurements on the $Cr_2Ge_2Te_6$ single crystal with NaCl used as the PTM, well consistent with the DFT calculations. The observed onset of metallization pressure of $Cr_2Ge_2Te_6$ takes place at considerably lower pressures than previous reports of 7–14 GPa. Our powder x-ray diffraction measurements using NaCl as the PTM reveal the absence of the phase transition of $Cr_2Ge_2Te_6$ at 3.9 GPa, hence the metallization of the sample is intrinsically from its electronic changes under compression. The distinct band-gap closure demonstrates compression-induced electronic changes in this 2D material as a consequence of the

contraction of Cr-Te bonds lengths. Unlike the isostructural $Cr_2Si_2Te_6$, we did not observe superconductivity down to 2.4 K in the whole crystalline phase region. This study sheds light on the interplay between crystal structure and electronic properties of layered 2D materials and demonstrates the phase stability and metallization in this system may be strongly related to the different hydrostatic environments.

ACKNOWLEDGMENTS

W.C. would like to acknowledge the startup funding provided by University of Electronic Science and Technology of China. We thank Jiangang He for fruitful discussions. We thank A. Dockery, A. Glende, F. Safari, M. Burden, I. Saffarian-Deemyad, J. St. Andre, and T. McNamee for help with high-pressure x-ray data collection. The authors would like to acknowledge S. Tkachev for the assistance of helium gas loading for the single-crystal x-ray measurements and J. Smith and C. Kenney-Benson for providing experimental support at HPCAT. The high-pressure single-crystal x-ray diffraction data and powder x-ray diffraction data were collected at 13-BM-C of GeoSoilEnviroCARS (The University of Chicago, Sector 13) and at 16-ID-B of HP-CAT (Sector 16), Advanced Photon Source (APS), Argonne National Laboratory, respectively. GeoSoilEnviroCARS is supported by the National Science Foundation-Earth Sciences (EAR-1634415) and Department of Energy-GeoSciences (DE-FG02-94ER14466). HPCAT operations are supported by DOE-NNSA's Office of Experimental Sciences. Use of the COMPRES-GSECARS gas loading system and PX2 was supported by COMPRES under NSF Cooperative Agreement EAR-1661511 and by GSECARS through NSF Grant No. EAR-1634415 and DOE Grant No. DE-FG02-94ER14466. Work at Argonne (sample preparation, characterization, and crystal growth) is supported by the U.S. DOE, Office of Basic Energy Science, Materials Science and Engineering Division. Use of the Advanced Photon Source at Argonne National Laboratory was supported by the U.S. Department of Energy, Office of Science, Office of Basic Energy Sciences, under Contract No. DE-AC02-06CH11357. Support from the University of Utah Office of Undergraduate Research and Physics & Astronomy Summer Undergraduate Research Program in the dissemination of the research is acknowledged.

[1] K. S. Burch, D. Mandrus, and J.-G. Park, Nature (London) **563**, 47 (2018).
[2] C. Felser, G. H. Fecher, and B. Balke, Angew. Chem., Int. Ed. **46**, 668 (2007).
[3] B. Huang, G. Clark, D. R. Klein, D. MacNeill, E. Navarro-Moratalla, K. L. Seyler, N. Wilson, M. A. McGuire, D. H. Cobden, D. Xiao *et al.*, Nat. Nanotechnol. **13**, 544 (2018).
[4] C. Gong, L. Li, Z. Li, H. Ji, A. Stern, Y. Xia, T. Cao, W. Bao, C. Wang, Y. Wang *et al.*, Nature (London) **546**, 265 (2017).
[5] M. A. McGuire, H. Dixit, V. R. Cooper, and B. C. Sales, Chem. Mater. **27**, 612 (2015).
[6] B. Huang, G. Clark, E. Navarro-Moratalla, D. R. Klein, R. Cheng, K. L. Seyler, D. Zhong, E. Schmidgall, M. A. McGuire, D. H. Cobden *et al.*, Nature (London) **546**, 270 (2017).
[7] J. F. Dillon and C. E. Olson, J. Appl. Phys. **36**, 1259 (1965).
[8] B. Siberchicot, S. Jobic, V. Carteaux, P. Gressier, and G. Ouvrard, J. Phys. Chem. **100**, 5863 (1996).
[9] V. Carteaux, F. Moussa, and M. Spiesser, Europhys. Lett. **29**, 251 (1995).
[10] G. Ouvrard, E. Sandre, and R. Brec, J. Solid State Chem. **73**, 27 (1988).
[11] V. Carteaux, D. Brunet, G. Ouvrard, and G. Andre, J. Phys.: Condens. Matter. **7**, 69 (1995).
[12] T. Li, S. Jiang, N. Sivadas, Z. Wang, Y. Xu, D. Weber, J. E. Goldberger, K. Watanabe, T. Taniguchi, C. J. Fennie *et al.*, Nat. Mater. **18**, 1303 (2019).
[13] T. Song, Z. Fei, M. Yankowitz, Z. Lin, Q. Jiang, K. Hwangbo, Q. Zhang, B. Sun, T. Taniguchi, K. Watanabe *et al.*, Nat. Mater. **18**, 1298 (2019).
[14] S. Mondal, M. Kannan, M. Das, L. Govindaraj, R. Singha, B. Satpati, S. Arumugam, and P. Mandal, Phys. Rev. B **99**, 180407(R) (2019).
[15] W. Cai, H. Sun, W. Xia, C. Wu, Y. Liu, H. Liu, Y. Gong, D.-X. Yao, Y. Guo, and M. Wang, Phys. Rev. B **102**, 144525 (2020).
[16] D. Bhoi, J. Gouchi, N. Hiraoka, Y. Zhang, N. Ogita, T. Hasegawa, K. Kitagawa, H. Takagi, K. H. Kim, and Y. Uwatoko, Phys. Rev. Lett. **127**, 217203 (2021).
[17] Y. Sun, R. C. Xiao, G. T. Lin, R. R. Zhang, L. S. Ling, Z. W. Ma, X. Luo, W. J. Lu, Y. P. Sun, and Z. G. Sheng, Appl. Phys. Lett. **112**, 072409 (2018).
[18] Z. Lin, M. Lohmann, Z. A. Ali, C. Tang, J. Li, W. Xing, J. Zhong, S. Jia, W. Han, S. Coh *et al.*, Phys. Rev. Materials **2**, 051004(R) (2018).
[19] A. O. Fumega, S. Blanco-Canosa, H. Babu-Vasili, P. Gargiani, H. Li, J.-S. Zhou, F. Rivadulla, and V. Pardo, J. Mater. Chem. C. **8**, 13582 (2020).
[20] W. Ge, K. Xu, W. Xia, Z. Yu, H. Wang, X. Liu, J. Zhao, X. Wang, N. Yu, Z. Zou *et al.*, J. Alloys Compd. **819**, 153368 (2020).
[21] E. Dong, B. Liu, Q. Dong, X. Shi, X. Ma, R. Liu, X. Zhu, X. Luo, X. Li, Y. Li *et al.*, Phys. B (Amsterdam, Neth.) **595**, 412344 (2020).
[22] Z. Yu, W. Xia, K. Xu, M. Xu, H. Wang, X. Wang, N. Yu, Z. Zou, J. Zhao, L. Wang *et al.*, J. Phys. Chem. C **123**, 13885 (2019).
[23] H. Ji, R. A. Stokes, L. D. Alegria, E. C. Blomberg, M. A. Tanatar, A. Reijnders, L. M. Schoop, T. Liang, R. Prozorov, K. S. Burch *et al.*, J. Appl. Phys. **114**, 114907 (2013).
[24] H. K. Mao, R. J. Hemley, Y. Wu, A. P. Jephcoat, L. W. Finger, C. S. Zha, and W. A. Bassett, Phys. Rev. Lett. **60**, 2649 (1988).
[25] W. Cai, M. T. Hossain, J. Coles, J. Lybarger, J. Blanton, E. Sterer, and S. Deemyad, High Press. Res. **39**, 628 (2019).
[26] G. Sheldrick, Acta Crystallogr., Sect. A: Found. Crystallogr. **64**, 112 (2008).
[27] O. V. Dolomanov, L. J. Bourhis, R. J. Gildea, J. A. K. Howard, and H. Puschmann, J. Appl. Crystallogr. **42**, 339 (2009).
[28] See Supplemental Material at http://link.aps.org/supplemental/10.1103/PhysRevB.106.085116 for detailed structure information and electrical transport measurements data at various pressures.

[29] C. Prescher and V. B. Prakapenka, High. Press. Res. **35**, 223 (2015).
[30] B. Toby, J. Appl. Crystallogr. **34**, 210 (2001).
[31] G. Kresse and J. Furthmüller, Phys. Rev. B **54**, 11169 (1996).
[32] P. E. Blöchl, Phys. Rev. B **50**, 17953 (1994).
[33] P. E. Blöchl, O. Jepsen, and O. K. Andersen, Phys. Rev. B **49**, 16223 (1994).
[34] J. P. Perdew, K. Burke, and M. Ernzerhof, Phys. Rev. Lett. **77**, 3865 (1996).
[35] Y. Fang, S. Wu, Z.-Z. Zhu, and G.-Y. Guo, Phys. Rev. B **98**, 125416 (2018).
[36] A. D. Becke and K. E. Edgecombe, J. Chem. Phys. **92**, 5397 (1990).
[37] S. Klotz, J. C. Chervin, P. Munsch, and G. L. Marchand, J. Phys. D: Appl. Phys. **42**, 075413 (2009).
[38] L. Zhang, Y. Tang, A. R. Khan, M. M. Hasan, P. Wang, H. Yan, T. Yildirim, J. F. Torres, G. P. Neupane, Y. Zhang *et al.*, Adv. Sci. **7**, 2002697 (2020).
[39] W. Cai, J. He, H. Li, R. Zhang, D. Zhang, D. Y. Chung, T. Bhowmick, C. Wolverton, M. G. Kanatzidis, and S. Deemyad, Nat. Commun. **12**, 1509 (2021).
[40] K. Xu, Z. Yu, W. Xia, M. Xu, X. Mai, L. Wang, Y. Guo, X. Miao, and M. Xu, J. Phys. Chem. C. **124**, 15600 (2020).
[41] Y. Liu and C. Petrovic, Phys. Rev. B **96**, 054406 (2017).
[42] T. Varga, A. P. Wilkinson, and R. J. Angel, Rev. Sci. Instrum. **74**, 4564 (2003).
[43] V. A. Sidorov and R. A. Sadykov, J. Phys.: Condens. Matter **17**, S3005 (2005).
[44] P. Kuiper, G. Kruizinga, J. Ghijsen, G. A. Sawatzky, and H. Verweij, Phys. Rev. Lett. **62**, 221 (1989).
[45] H.-S. Kim, K. Haule, and D. Vanderbilt, Phys. Rev. Lett. **123**, 236401 (2019).